On-surface design of a 2D transition metal-organic network preserving large orbital magnetic moment

C. Martín-Fuentes[1,‡], S. O. Parreiras[1,*,‡], J. I. Urgel[1], V. Rubio-Giménez[2,+], B. Muñiz-Cano[1], D. Moreno[1], K. Lauwaet[1], M. Valvidares[3], M. A. Valbuena[1], P. Gargiani[3], Wolfgang Kuch[4], J. Camarero[1,5], J. M. Gallego[6], R. Miranda[1,5], J. I. Martínez[6,*], C. Martí-Gastaldo[2,*], and D. Écija[1,*]

[1]Instituto Madrileño de Estudios Avanzados en Nanociencia (IMDEA Nanoscience), E-28049 Madrid, Spain

[2]Instituto de Ciencia Molecular (ICMol), Universitat de València, 46980 Paterna, Spain

[3]ALBA Synchrotron Light Source, E-08290, Barcelona, Spain

[4]Institut für Experimentalphysik, Freie Universität Berlin, 14195 Berlin, Germany

[5]Departamento de Física de la Materia Condensada and Condensed Matter Physics Center (IFIMAC), Universidad Autónoma de Madrid, Cantoblanco, 28049 Madrid, Spain

[6]Instituto de Ciencia de Materiales de Madrid (ICMM-CSIC), Cantoblanco, 28049 Madrid, Spain

ABSTRACT: The design of antiferromagnetic nanomaterials preserving large orbital magnetic moment is important to protect their functionalities against magnetic perturbations. Here, we exploit an archetype H_6HOTP species for conductive metal-organic frameworks to design a Co-HOTP one-atom thick metal-organic architecture on an Au(111) surface. Our multidisciplinary scanning probe microscopy, X-ray absorption spectroscopy, X-ray linear dichroism and X-ray magnetic circular dichroism study, combined with density functional theory simulations, reveals the formation of a unique network design based on three-fold Co^{+2} coordination with deprotonated ligands, which displays large orbital magnetic moment with an orbital to effective spin moment ratio of 0.8, in-plane easy axis of magnetization and large magnetic anisotropy. Our simulations suggest an antiferromagnetic ground state, which is compatible with our experimental findings. Such Co-HOTP metal-organic network exemplifies how on-surface chemistry can enable the design of field-robust antiferromagnetic materials.

INTRODUCTION

Magnetic anisotropy is a fundamental property in magnetism responsible for the preferential directions of magnetization. Atomistically, the spin-orbit coupling connects the spin and the orbital magnetic moment of a material. This, together with the orbital anisotropy, gives rise to the magnetic anisotropy. According to Hund's rules, free transition metal atoms can possess large orbital magnetic moments. However, whenever such atoms are located in a solid, crystal field effects typically split the energy degeneracy of *d*-orbitals, which causes partial or total quenching of the orbital magnetic moment.[1] Enormous efforts have been devoted to overcome such limitations, mostly centered on reducing the coordination of the transition metal in order to increase the orbital magnetic moment and, thus, to enhance the magnetic anisotropy. However, these efforts have been mainly concentrated in controlling local coordination environments of discrete molecules[1-7] whereas the route to comparable control in extended solids remains still blocked. In this regard, the design of antiferromagnetic solids is particularly relevant in spintronics because of their robustness against perturbations from magnetic fields, while not producing stray fields.[8,9] Herein, the magnetic anisotropy is one of the key parameters that determines the degree of protection. The capability to preserve a large orbital magnetic moment in two-dimensional metal-organic networks[10-12] is crucial to steer spin-orbit coupling and to enhance the magnetic anisotropy. A large magnetic anisotropy has been theoretically predicted for some 2D metal-organic systems;[13-16] however, the experimental achievement of such systems has remained elusive.

Metal-Organic Frameworks (MOFs) have emerged as molecule-based architectures with chemical and structural versatilities not comparable to any other synthetic material.[17] The last decade has witnessed how the synthetic control over metal nodes and organic ligands has enabled the design of materials for targeted applications in fields as diverse as sensing, gas storage/separation, catalysis, light emission, energy harvesting or magnetism.[17-23] This chemical diversity and structural tunability has also been a central tool for engineering the properties of two-dimensional conjugated metal-organic frameworks (2D c-MOFs).[24] Such metal-organic nanomaterials are built from the packing of layers formed by transition metal ions coordinated to -NH_2, -OH, -SH or -SeH functional groups with single/polyaromatic cores, and predominantly crystallize in porous hexagonal honeycomb lattices, whilst there are only a handful of examples of dense Kagome networks with benzene and coronene-based ligands. From a physical standpoint, chemical control of these systems can allow for augmented mobility of the charge carriers due to extended intralayer conjugation,[24-26] or allow the expression of novel quantum phases of matter.[27-31] The possibility of confining their

growth to just atomically-thick 2D layers by using an on-surface chemistry approach offers exciting opportunities for investigating their electronic and magnetic properties at the ultimate spatial resolution,[32-34] which now we contribute to extend to the assembly of topologies and metal coordination indexes only accessible in solvent-free environments.[35-37]

Here, we carried out a multidisciplinary study combining scanning tunnelling microscopy (STM) and spectroscopy (STS), non-contact atomic force microscopy (nc-AFM), X-ray adsorption spectroscopy (XAS), X-ray linear dichroism (XLD), X-ray magnetic circular dichroism (XMCD) and density functional theory complemented by a Hubbard model (DFT+U), to illustrate the on-surface synthesis of an unprecedent Co-HOTP metal-organic network on Au(111) based on the deprotonation of H_6HOTP (2,3,6,7,10,11-hexahydroxytriphenylene) species and their subsequent coordination with cobalt (Co) atoms. The Co-HOTP architecture displays a large orbital magnetic moment with an orbital to effective spin moment ratio of 0.8, in-plane easy axis of magnetization and large magnetic anisotropy. Our density functional calculations predict the antiferromagnetic nature of the coordinative assembly, which agrees with the XLD/XMCD results. Thus, our findings illustrate avenues to engineer field-robust antiferromagnetic materials.

RESULTS AND DISCUSSION

The deposition of a submonolayer coverage of 2,3,6,7,10,11-hexahydroxytriphenylene (H_6HOTP)[38-41] (cf. left panel of Figure 1a and Figures SI1,2) on a clean Au(111) surface and further annealing to 250 °C, gives rise to a disordered self-assembled architecture coexisting with ordered patches, based on hydrogen bonds and van der Waals interactions between adjacent molecules (cf. Figure SI3).

This scenario changes in the presence of Co adatoms. The sublimation of Co on a submonolayer coverage of H_6HOTP on Au(111) held at 100 °C, and its subsequent annealing to 250 °C, results in the formation of long-range supramolecular islands with rounded borders (cf. Figure SI4). For sufficient Co dosage, no sign of the pristine H_6HOTP architecture is detected. Instead, a novel Co-directed metal-organic network is formed, to be termed Co-HOTP, thanks to the full deprotonation of the linkers[38] and the subsequent formation of Co-O bonds (cf. Figure 1a).

Such assembly is different from the previously reported 2D honeycomb $Co_3(HOTP)_2$ layers in cobalt-directed 2D c-MOFs synthesized in wet chemistry[38] which illustrates the crucial role of surface confinement. The confinement in 2D, the interaction of the adsorbates with the surface and the presence of high symmetry directions direct the growth favouring specific coordination symmetries. High-resolution STM images allow to discern two molecular orientations of the molecular species per domain, related by a 60º rotation, featuring a packed assembly with two distinct small pores (cf. Figure 1b,c). Notably, nc-AFM reveals the nature of the bonds (cf. Figure 1d), which are three-fold Co-O links, with a mean average projected bond distance of 1.91 Å. Importantly, one species displays a four-fold coordination, whereas the other one features a six-fold coordinative scheme (see Figures SI5 and SI7), resulting in an overall periodic metal-organic architecture.

On the basis of the experimental observations, we have performed DFT+U-based calculations to obtain a fully-relaxed interfacial structure. In the ground state configuration (cf. discussion below), the molecular ligands forming the network lie flat at 3.3-3.4 Å above the Au surface, whilst the coordinative Co atoms are located at 2.8 Å and 3.2 Å above the surface. The relaxed structure yields Co-O bond-lengths ranging from 1.86 Å to 1.92 Å, in excellent agreement with the experimental evidence from nc-AFM images (cf. Figure 1d). In addition, the simulated nc-AFM images match very well with the experimental ones, ratifying the rationalization of the self-assembly (cf. Figure 1e).

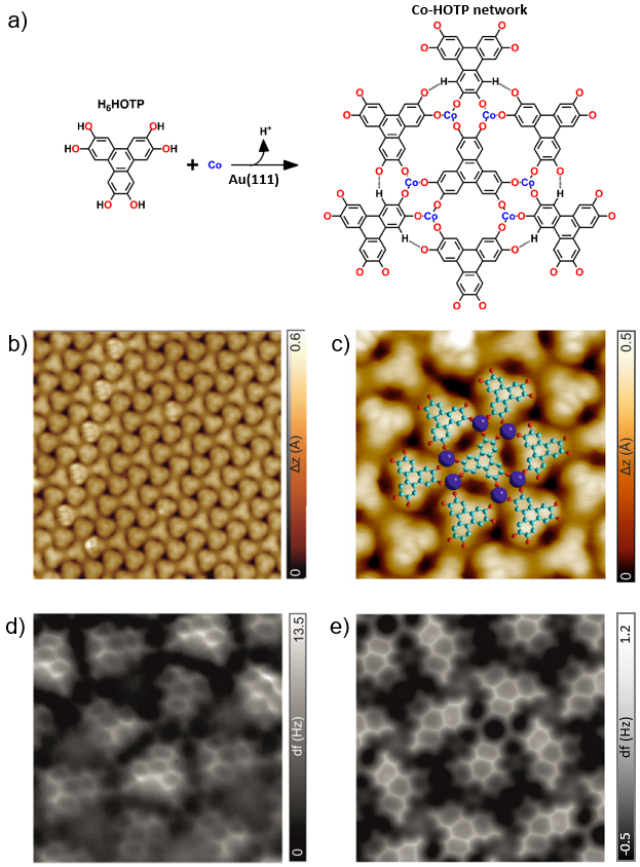

Figure 1. On-surface design of Co-HOTP network on Au(111). (a) Synthetic route toward the design of Co-HOTP on Au(111). (b) Mid-range STM image of the coordinative architecture. (c) High resolution STM image with a superimposed ball and stick model. Cyan, red, violet and white spheres depict carbon, oxygen, cobalt and hydrogen atoms, respectively. (d) Constant-height frequency-shift nc-AFM image acquired with a CO-functionalized tip. (e) nc-AFM simulation of (d). Image size: (b) 11.7 nm x 11.7 nm; (c) 4 nm x 4 nm; (d-e) 3.2 nm x 3.2 nm. STM parameters: (b) V_b = 20 mV, I_t = 120 pA, T = 4 K; (c) V_b = 20 mV, I_t = 100 pA, T = 4 K; (d) Open feedback: V_b = 5mV, I_t = 150 pA, Z_{offset} = 150 pm, T = 4 K.

The magnetic ground state has been calculated starting from several geometrical models and spin states accounting for spin-orbit coupling and non-collinear spin effects (see further details in the Supplementary Information). As illustrated in Figure 2, we have computed the energy of the following interfacial spin-configurations: i) spin-unpolarized case, ii) ferro- and antiferromagnetic out-of-plane spin couplings, and iii) distinct in-equivalent in-plane spin cases.

Such calculations reveal that the most energetically favourable configuration for both free-standing (cf. Figure SI6) and surface-confined network corresponds to the local non-collinear antiferromagnetic state with all spins in-plane (highlighted in Figure 2 by a red square) and with Co atoms featuring a +2 oxidation state.

We have inspected by DFT+U the electronic structure of the spin ground state configuration (red square in Figure 2) of the interfacial

network, where U has been taken in this case to be 3.75 eV, a value optimized for Co^{+2}.[42] Our results shown in Figure 3a display an electronic gap of 30 meV at the K point and band extrema at the Γ point located at -0.15 eV and 0.10 eV, respectively.

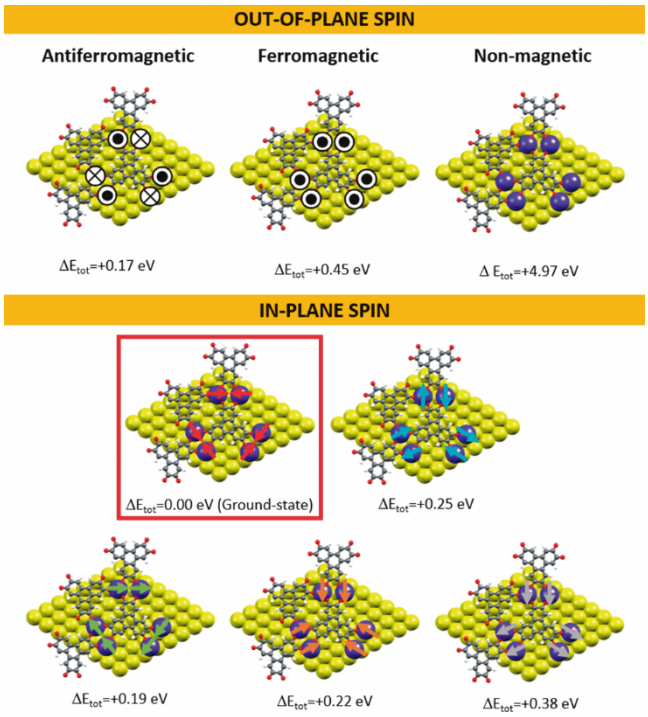

Figure 2. Schematic top view of the (fully structurally and electronically relaxed) different interfacial spin configurations considered in the calculations including both the Co-HOTP network and the Au substrate to elucidate the spin ground-state: (top) antiferromagnetic, ferromagnetic and spin-unpolarized out-of-plane spin cases; and (bottom) representative inequivalent in-plane spin configurations. The red square highlights the ground-state.

In order to experimentally probe the electronic structure of the Co-HOTP, we have performed scanning tunnelling spectroscopy at selected positions on the network and on Au(111). Notably, there are weak features located on the 4-fold and 6-fold coordinated molecular species at ~ -0.21 eV and ~ +0.07 eV, as well as on Co atoms at ~ -0.16 eV and ~ +0.13 eV (cf. Fig. 3b). These features might reflect the predicted band extrema at the Γ point. The linear decrease in the DOS leading to a minimum at the Fermi level might be consistent with the very small gap predicted by theory. Such bandgap is significantly smaller than the one reported in $Co_3(HOTP)_2$ frameworks.[43]

Next, we performed XAS, XMCD and XLD measurements. Figure 4a presents XAS/XMCD spectra taken at Co $L_{2,3}$-edges at grazing (GI = 70°) and normal (NI = 0°) incidences, measured at 2 K and 6 T. The L_3-XAS spectra present a multiplet peak structure indicative of strong localization of Co-3*d* electrons, which is consistent with a +2 oxidation state for Co (cf. discussion in Supporting Information, Figure SI8),[44-47] in agreement with the results of DFT+U calculations. Further, the XMCD signal has the same negative sign at both L_3 and L_2-edges at GI, whereas L_2 vanishes at NI, both of them characteristic of a very large orbital moment. The XMCD is much larger at grazing incidence, i.e., a strong anisotropy with an in-plane easy axis is observed.

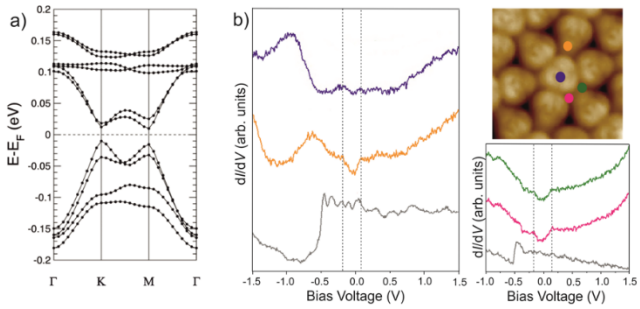

Figure 3. Electronic structure of the Co-HOTP network on Au(111). (a) Computed DFT+U (U=3.75 eV for Co^{+2}) electronic band structure for the network ground-state spin-configuration of Figure 2. The zero energy is taken to correspond to the Fermi energy, whilst the x-axis labels denote a path through the 3D space of the k-vectors. Points of high-symmetry in the Brillouin zone are labelled as Γ(0,0,0), M(0,1/2,0) and K(1/3,2/3,0), all in reciprocal space coordinates. (b) dI/dV spectra on representative positions of the metal-organic network (marked with colored circles in the STM image). STS spectra acquired on clean Au(111) are depicted in grey. Image size: 5 nm x 5 nm. STM parameters: V_b = 300 mV, I_t = 300 pA, T = 4 K.

Table 1 displays the expectation values of effective spin ($\langle S_{eff} \rangle$) and orbital ($\langle L_z \rangle$) operators in $\hbar$ units, and effective spin ($m_{eff} = 2\langle S_{eff} \rangle$), orbital ($m_l$) magnetic moments in μ_B, and the orbital to effective spin moment ratio ($\langle L_z \rangle / 2\langle S_{eff} \rangle$) calculated by sum rules.[48,49] These values are actually the expectation values of the magnetic moments projected onto the X-ray incidence direction at the experimental conditions of 6 T and 2 K. Here, it is worth to point out that the real magnetic moments can only be probed at full saturation, which is not the case (see discussion below), and, thus, in such scenarios, the expectation values of the moments represent a lower limit for the real magnetic moments.

Table 1. Effective spin ($\langle \boldsymbol{S_{eff}} \rangle$) and orbital ($\langle \boldsymbol{L_z} \rangle$) operators in $\hbar$ units, effective spin ($\boldsymbol{m_{S_{eff}}}$) and orbital ($\boldsymbol{m_L}$) moments in μ_B, and orbital to effective spin moment ratio ($\langle \boldsymbol{L_z} \rangle / \boldsymbol{2\langle S_{eff} \rangle}$) extracted by XMCD sum rules for grazing (70°) and normal (0°) incidences at 6 T and 2 K for Co centers on Co-HOTP networks in Au(111).

Incidence angle (°)	$\langle S_{eff} \rangle$ ($\hbar$)	$\langle L_z \rangle$ ($\hbar$)	$m_{S_{eff}}$ (μ_B)	m_L (μ_B)	$\langle L_z \rangle / 2\langle S_{eff} \rangle$
70	0.61 (6)	0.98 (10)	1.22 (12)	0.98 (10)	0.80(11)
0	0.14 (1)	0.19 (2)	0.28 (3)	0.19 (2)	0.68(10)

At NI the small magnetic dichroism reflects that the expectation values of the magnetic moments are very low. At GI, on the other side, the XMCD presents high intensity and large moments. The in-plane orbital moment is 0.98 μ_B, which is an exceptionally large and unprecedented value for a 3*d* metal in 2D metal-organic networks.

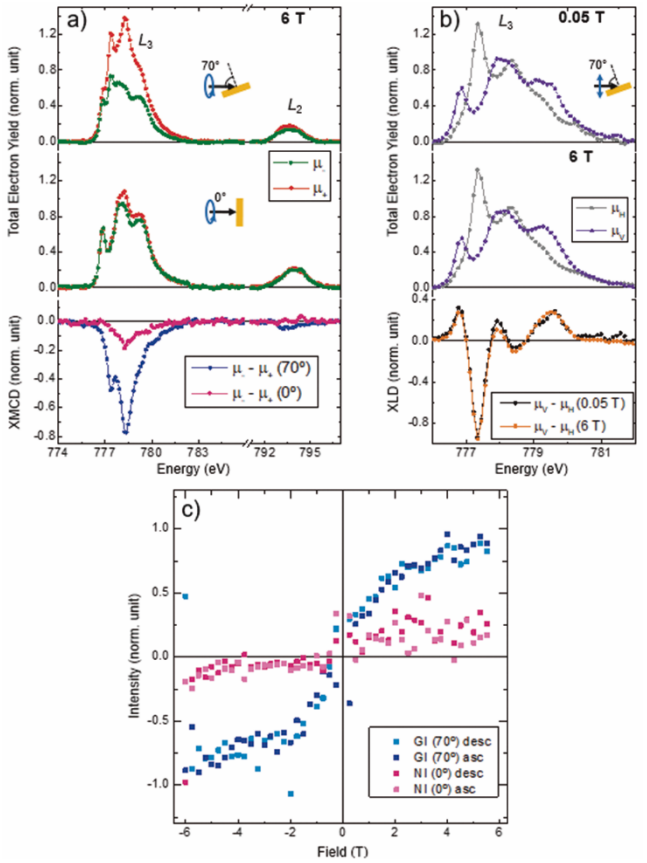

Figure 4. Magnetic properties of Co-HOTP network on Au(111). (a) XAS spectra with positive (μ_+, red) and negative (μ_-, green) circularly polarized light and XMCD ($\mu_- - \mu_+$) taken at the Co $L_{2,3}$ edges at grazing (70°, blue) and normal (0°, pink) incidences (B = 6 T, T = 2 K). (b) XAS spectra acquired with vertical (μ_V, purple) and horizontal (μ_H, grey) linearly polarized light and XLD ($\mu_V - \mu_H$) taken at Co L_3-edge at grazing (70°) incidence for fields of 0.05 T (black) and 6 T (orange) (T = 2 K). (c) Magnetization curves constructed by measuring the XMCD intensity at the highest peak of Co L_3-edge at grazing (70°, blue) and normal (0°, pink) incidences. Dark (light) dots represent the descending (ascending) branches (T = 2 K).

For the spin moment, our DFT+U calculations determine an average spin quantum number $\langle S_z \rangle = 0.95$ for the Co atoms (cf. Figure SI9 and discussion in Supplementary Information). The sum rules determine the effective spin ($\langle S_{eff} \rangle = \langle S_z \rangle + 7/2 \langle T_z \rangle$), whereby the dipole term ($\langle T_z \rangle$) can be significant in systems with low symmetry. In Co porphyrins, for instance, the dipole moment was found to have an inverted sign and a larger magnitude than the spin moment for some angles.[50] From the sum-rules analysis, Co-HOTP networks have an $\langle S_{eff} \rangle = 0.61$ (6) at GI, 6 T and 2 K. The impossibility of reaching saturation hinders the determination of the dipole term by angle dependent measurements, so, based on the experimental data, it is not possible to unequivocally infer the spin state. Herein, it is worth to note that the real $\langle S_{eff} \rangle$ at full saturation could be larger and the dipole term could be negative, which would bring the experimental $\langle S_z \rangle$ into agreement with the calculation.

Notably, a very large orbital to effective spin moment ratio ($\langle L_z \rangle / 2 \langle S_{eff} \rangle$) is observed. Such ratio is obtained from XMCD alone and without assumptions on number of holes, which makes it very robust with respect to background subtraction. Notice that this ratio is close to the ones reported in the case of 3*d* adatoms on top of metallic alkali surfaces.[51] The ratio of orbital to effective spin magnetic moment changes from 0.80 to 0.68 between GI and NI. Because of the unknown contribution of the dipole term, no direct conclusion about the anisotropy of the orbital moment can be drawn from these numbers. However, since the $\langle T_z \rangle$ term enters with opposite sign in the two measurements,[50] the ratio of orbital to spin moment is either in between these two values, or > 0.80 for GI and < 0.68 for NI. In any case, these are extraordinarily high values for transition-metal coordination networks.

XLD spectra at low magnetic field (0.05 T, see Figure 4b) feature a giant anisotropy, with more than 90% of dichroism. This is an indication of strong charge density anisotropy due to the coordinative crystal field. Consequently, any possible magnetic contribution to the XLD is hidden by the charge effect and when a 6 T field is applied, the shape of XLD is similar only with subtle differences in the peak's intensity.

Magnetization curves for GI and NI are shown in Figure 4c. For NI the curve is almost linear with low intensity even at 6 T. In the case of GI, a larger susceptibility and some curvature are observed. However, it is worth noting that also in the case of GI the magnetization curve is not at saturation, possibly indicating the presence of antiferromagnetic interactions among Co moments. These results together with the XLD/XMCD findings are compatible with a weak antiferromagnetism, as predicted by DFT+U.

CONCLUSIONS

In summary, we report the on-surface synthesis of a Co-HOTP metal-organic network on Au(111) based on the coordination of H_6HOTP species with Co upon thermal activation of OH groups. The resulting coordinative pattern relies on 4-fold and 6-fold coordinative species, giving rise altogether to a unique periodic architecture, which illustrates the power of surface-confined metal-organic chemistry to design unparalleled low dimensional architectures. A comprehensive STS study, complemented by DFT+U calculations, reveals that the network features a very low bandgap. Our calculations illustrate that the coordinative architecture displays an antiferromagnetic ground state, with Co presenting a +2 oxidation state. Such findings are compatible with our XAS, XLD and XMCD investigations. As result of its low coordination index, cobalt atoms exhibit a large unquenched orbital magnetic moment and a large orbital to effective spin moment ratio unprecedented in 2D coordinative architectures based on 3d metals. We are confident our results open new pathways for the engineering of antiferromagnetic low dimensional materials featuring strong anisotropy, of great relevance in potential spintronic and memory devices.

ASSOCIATED CONTENT

Supporting Information

Synthesis of H_6HOTP species.
Experimental methods.
Theoretical framework and computational details.
Lattice geometry and crystal field.
Oxidation state of Co in the Co-HOTP networks.
Calculations of spin quantum number.
Calculation of the exchange interaction (J).
The Supporting Information is available free of charge on the ACS Publications website.

AUTHOR INFORMATION

Corresponding Author

SOP: sofia.oliveira@imdea.org
JIM: joseignacio.martínez@icmm.csic.es
CMG: carlos.marti@uv.es
DE: david.ecija@imdea.org

Present Address

+Centre for Membrane Separations, Adsorption, Catalysis, and Spectroscopy (cMACS), KU Leuven, Celestijnenlaan 200F, 3001 Leuven, Belgium.

Author Contributions

The manuscript was written through contributions of all authors.
All authors have given approval to the final version of the manuscript.
‡These authors contributed equally.

Notes

The authors declare no competing financial interests.

ACKNOWLEDGMENT

This project has received funding from the European Research Council (ERC, grant 766555) and Marie Sklodowska-Curie Actions (MSCA, project 894924) under the European Union's Horizon 2020 research and innovation program, from Spanish MINECO (MAT2017-85089-C2-1-R, PID2019-108532GB-I00 and PID2020-118117RB-I00), from Comunidad Autónoma de Madrid via 'Programa de Investigación Tecnologías' 2018 (FOTOART-CM S2018/NMT-4367, NANOMAGCOST-CM S2018/NMT-4321) and the Generalitat Valenciana (PROMETEU/2021/054). IMDEA Nanociencia and ICMol acknowledge support from the 'Severo Ochoa' and 'María de Maeztu' Programs for Centers of Excellence in R&D (MINECO, Grant SEV-2016-0686 and CEX2019-000919-M). The ALBA synchrotron is acknowledged for providing beam time at BOREAS beamline (proposal number 2020094657).

REFERENCES

1. Guirado-López, R. A.; Dorantes-Dávila, J.; Pastor, G. M., Orbital Magnetism in Transition-Metal Clusters: From Hund's Rules to Bulk Quenching. *Phys. Rev. Lett.* **2003**, *90*, 226402.
2. Gambardella, P.; Rusponi, S.; Veronese, M.; Dhesi, S. S.; Grazioli, C.; Dallmeyer, A.; Cabria, I.; Zeller, R., Giant Magnetic Anisotropy of Single Cobalt Atoms and Nanoparticles. *Science* **2003**, *300*, 1130-1133.
3. Autès, G.; Barreteau, C.; Spanjaard, D.; Desjonqueres, M.-C.; Dederichs, P. H.; Kern, K.; Carbone, C.; Brune, Magnetism of iron: from the bulk to the monoatomic wire. *J. Phys.: Condens. Matter* **2006**, *18*, 6785-6813.
4. H.; Zadrozny, J. M.; Xiao, D. J.; Atanasov, M.; Long, G. J.; Grandjean, F.; Neese, F.; Long, J. R., Magnetic blocking in a linear iron(I) complex. *Nat. Chem.* **2013**, *5*, 577-581.
5. Langenberg, A.; Hirsch, K.; Ławicki, A.; Zamudio-Bayer, V.; Niemeyer, M.; Chmiela, P.; Langbehn, B.; Terasaki, A.; Issendorff, B. v.; Lau, J. T., Spin and orbital magnetic moments of size-selected iron, cobalt, and nickel clusters. *Phys. Rev. B* **2014**, *90*, 184420.
6. Rau, I. G.; Baumann, S.; Rusponi, S.; Donati, F.; Stepanow, S.; Gragnaniello, L.; Dreiser, J.; Piamonteze, C.; Nolting, F.; Gangopadhyay, S.; Albertini, O. R.; Macfarlane, R. M.; Lutz, C. P.; Jones, B. A.; Gambardella, P.; Heinrich, A. J.; Brune, H., Reaching the magnetic anisotropy limit of a 3d metal atom. *Science* **2014**, *344*, 988-992.
7. Bunting, P. C.; Atanasov, M.; Damgaard-Møller, E., Perfetti, M.; Crassee, I.; Orlita, M.; Overgaard, J.; van Slageren, J.; Neese, F.; Long, J. R., A linear cobalt(II) complex with maximal orbital angular momentum from a non-Aufbau ground state. *Science* **2018**, *362*, 1378.
8. Jungwirth, T.; Marti, X.; Wadley, P.; Wunderlich, J., Antiferromagnetic spintronics. *Nat. Nanotechnol.* **2016**, *11*, 231-241.
9. Baltz, V.; Manchon, A.; Tso, M.; T. Moriyama, Ono, T.; Tserkovnyak, Antiferromagnetic spintronics. Y., *Rev. Mod. Phys.* **2018**, *90*, 015005.
10. Gambardella, P.; Stepanow, S.; Dmitriev, A.; Honolka, J.; de Groot, F. M. F.; Lingenfelder, M.; Gupta, S. S.; Sarma, D. D.; Bencok, P.; Stanescu, S.; Clair, S.; Pons, S.; Lin, N.; Seitsonen, A. P.; Brune, H.; Barth, J. V.; Kern, K, Supramolecular control of the magnetic anisotropy in two-dimensional high-spin Fe arrays at a metal interface. *Nat. Mater.* **2009**, *8*, 189-193.
11. Abdurakhmanova, N.; Tseng, T.-C.; Langner, A.; Kley, C. S.; Sessi, V.; Stepanow, S.; Kern, K, Superexchange-Mediated Ferromagnetic Coupling in Two-Dimensional Ni-TCNQ Networks on Metal Surfaces. *Phys. Rev. Lett.* **2013**, *110*, 027202.
12. Faraggi, M. N.; Golovach, V. N.; Stepanow, S.; Tseng, T.-C.; Abdurakhmanova, N.; Kley, C. S.; Langner, A.; Sessi, V.; Kern, K.; Arnau, A., Modeling Ferro- and Antiferromagnetic Interactions in Metal–Organic Coordination Networks. *J. Phys. Chem. C* **2015**, *119*, 547-555.
13. Xing, J.; Wang, P.; Jiang, Z.; Jiang, X.; Wang, Y.; Zhao, J., Rational design of 2D organic magnets with giant magnetic anisotropy based on two-coordinate 5d transition metals. *APL Mater.* **2020**, *8*, 071105.
14. Wang, P.; Jiang, X.; Hu, J.; Zhao, J., Chemically Engineering Magnetic Anisotropy of 2D Metalloporphyrin. *Adv. Sci.* **2017**, *4*, 1700019.
15. Wang, P.; Jiang, X.; Hu, J.; Huangc, X., Zhao, J., Giant magnetic anisotropy of a 5d transition metal decorated two-dimensional polyphthalocyanine framework. *J. Mater. Chem. C* **2016**, *4*, 2147.
16. Wang, P.; Jiang, X.; Hu, J.; Wang, B.; Zhou, T.; Yuan, H.; Zhao, J., Robust spin manipulation in 2D organometallic Kagome lattices: a first-principles study. *Phys. Chem. Chem. Phys.* **2020**, *22*, 11045.
17. Furukawa, H.; Cordova, K. E.; O'keeffeand, M.; Yaghi, O. M., The chemistry and applications of metal-organic frameworks. *Science* **2013**, *341*, 1230444.
18. Cadiau, A.; Adil, K.; Bhatt, P. M.; Belmabkhout, Y.; Eddaoudi, M., A metal-organic framework–based splitter for separating propylene from propane. *Science* **2016**, *353*, 137-140.
19. Kim, E. J.; Siegelman, R. L.; Jiang, H. Z. H.; Forse, A. C.; Lee, J.-H.; Martell, J. D.; Milner, P. J.; Falkowski, J. M.; Neaton, J. B.; Reimer, J. A.; Weston, S. C.; Long, J. R., Cooperative carbon capture and steam regeneration with tetraamine-appended metal–organic frameworks. *Science* **2020**, *369*, 392-396.
20. Karmakar, A.; Samanta, P.; Desai, A. V.; Ghosh, S. K., Guest-Responsive Metal–Organic Frameworks as Scaffolds for Separation and Sensing Applications. Accounts of Chemical Research. *Acc. Chem. Res.* **2017**, *50*, 2457-2469.
21. Bavykina, A.; Kolobov, N.; Khan, I. S.; Bau, J. A.; Ramirez, A.; Gascon, J., Metal-Organic Frameworks in Heterogeneous Catalysis: Recent Progress, New Trends, and Future Perspectives. *Chem Rev* **2020**, *120*, 8468-8535.
22. Espallargas, G. M.; Coronado, E., Magnetic functionalities in MOFs: from the framework to the pore. *Chem. Soc. Rev.* **2018**, *47*, 533.
23. Lin, Z.-J.; Lü, J.; Hong, M.; Cao, R., Metal–organic frameworks based on flexible ligands (FL-MOFs): structures and applications. *Chem. Soc. Rev.* **2014**, *43*, 5867.

24. Wang, m.; Dong, R.; Feng, X., Two-dimensional conjugated metal–organic frameworks (2D c-MOFs): chemistry and function for MOFtronics. *Chem. Soc. Rev.* **2021**, *50*, 2764-2793.
25. Ko, M.; Mendecki, L.; Mirica, K. A., Conductive two-dimensional metal–organic frameworks as multifunctional materials. *Chem. Commun.*, **2018**, *54*, 7873-7891.
26. Xie, L. S.; Skorupskii, G.; Dincă, M., Electrically Conductive Metal–Organic Frameworks. *Chem. Rev.* **2020**, *120*, 8536-8580.
27. Huang, X.; Zhang, S.; Liu, L.; Yu, L.; Chen, G.; Xu, W.; Zhu, D., Superconductivity in a Copper(II)-Based Coordination Polymer with Perfect Kagome Structure. *Angew. Chem. Int. Ed.* **2018**, *57*, 146-150.
28. Zhang, X.; Zhou, Y.; Cui, B.; Zhao, M.; Liu, F., Theoretical Discovery of a Superconducting Two-Dimensional Metal–Organic Framework. *Nano Lett.* **2017**, *17*, 6166-6170.
29. Dong, L.; Kim, Y.; Er, D.; Rappe, A. M.; Shenoy, V. B., Two-Dimensional π-Conjugated Covalent-Organic Frameworks as Quantum Anomalous Hall Topological Insulators. *Phys. Rev. Lett.* **2016**, *116*, 096601.
30. Yamada, M. G.; Soejima, T.; Tsuji, N.; Hirai, D.; Dincă, M.; Aoki, H., First-principles design of a half-filled flat band of the kagome lattice in two-dimensional metal-organic frameworks. *Phys. Rev. B.* **2016**, *94*, 081102.
31. Hua, M.; Xia, B.; Wang, M.; Li, E.; Liu, J.; Wu, T.; Wang, Y.; Li, R.; Ding, H.; Hu, J.; Wang, Y.; Zhu, J.; Zhao, W.; Lin, N., Highly Degenerate Ground States in a Frustrated Antiferromagnetic Kagome Lattice in a Two-Dimensional Metal–Organic Framework. *J. Phys. Chem. Lett.* **2021**, *12*, 3733.
32. Barth, J. V., Fresh perspectives for surface coordination chemistry. *Surf. Sci.* **2009**, *603*, 1533-1541.
33. Dong, L.; Gao, Z.; Lin, N., Self-assembly of metal–organic coordination structures on surfaces. *Prog. Surf. Sci.* **2016**, *91*, 101-135.
34. Liu, J.; Abel, M.; Lin, N., On-Surface Synthesis: A New Route Realizing Single-Layer Conjugated Metal–Organic Structures. *J. Phys. Chem. Lett.* **2022**, *13*, 1356-1365.
35. Zhang, R.; Liu, J.; Gao, Y.; Hua, M.; Xia, B.; Knecht, P.; Papageorgiou, A. C.; Reichert, J.; Barth, J. V.; Xu, H.; Huang, L.; Lin, N., On-surface Synthesis of a Semiconducting 2D Metal–Organic Framework Cu3(C6O6) Exhibiting Dispersive Electronic Bands. *Angew. Chem. Int. Ed.* **2020**, *59*, 2669-2673.
36. Meng, X.; Kolodzeiski, E.; Huang, X.; Timmer, A.; Lammers, B. S.; Gao, H.-Y.; Mönig, H.; Liu, L.; Xu, W.; Amirjalayer, S.; Zhu, D.; Fuchs, H., Tunable Thiolate Coordination Networks on Metal Surfaces. *ChemNanoMat* **2020**, *6*, 1479-1484.
37. Lischka, M.; Dong, R.; Wang, M.; Martsinovich, N.; Fritton, M.; Grossmann, L.; Heckl, W. M.; Feng, X.; Lackinger, M., Competitive Metal Coordination of Hexaaminotriphenylene on Cu(111) by Intrinsic Copper Versus Extrinsic Nickel Adatoms. *Chem.Eur.J.* **2019**, *25*, 1975-1983.
38. Hmadeh, M.; Lu, Z.; Liu, Z.; Gándara, F.; Furukawa, H.; Wan, S.; Augustyn, V.; Chang, R.; Liao, L.; Zhou, F.; Perre, E.; Ozolins, V.; Suenaga, K.; Duan, X.; Dunn, B.; Yamamto, Y.; Terasaki, O.; Yaghi, O. M., New Porous Crystals of Extended Metal-Catecholates. *Chem. Mater.* **2012**, *24*, 3511-3513.
39. Rochefort, A.; Vernisse, L.; Gómez-Herrero, A. C.; Sánchez-Sánchez, C.; Martín-Gago, J. A.; Chérioux, F.; Clair, S.; Coraux, J.; Martínez, J. I., Role of the Structure and Reactivity of Cu and Ag Surfaces in the Formation of a 2D Metal–Hexahydroxytriphenylene Network. *J. Phys. Chem. C* **2021**, *125*, 17333–17341.
40. Gómez-Herrero, A. C.; Sánchez-Sánchez, C.; Chérioux, F.; Martínez, J. I.; Abad, J.; Floreano, L.; Verdini, A.; Cossaro, A.; Mazaleyrat, E.; Guisset, V.; David, P.; Lisi, S.; Gago, J. A. M.; Coraux, J., Copper-assisted oxidation of catechols into quinone derivatives. *Chem. Sci.*, **2021**, *12*, 2257-2267.
41. Marele, A. C.; Corral, I.; Sanz, P.; Mas-Ballesté, R.; Zamora, F.; Yáñez, M.; Gómez-Rodríguez, J. M., Some Pictures of Alcoholic Dancing: From Simple to Complex Hydrogen-Bonded Networks Based on Polyalcohols. *J. Phys. Chem. C* **2013**, *117*, 4680-4690.
42. Capdevila-Cortada, M.; Łodziana, Z.; López, N., Performance of DFT+U Approaches in the Study of Catalytic Materials. *ACS Catal.* **2016**, *6*, 8370-8379.
43. Mähringer, A.; Jakowetz, A. C.; Rotter, J. M.; Bohn, B. J.; Stolarczyk, J. K.; Feldmann, J.; Bein, T.; Medina, D. D., Oriented Thin Films of Electroactive Triphenylene Catecholate-Based Two-Dimensional Metal–Organic Frameworks. *ACS Nano* **2019**, *13*, 6711-6719.
44. Hollmann, N.; Hu, Z.; Valldor, M.; Maignan, A.; Tanaka, A.; Hsieh, H. H.; Lin, H.-J.; Chen, C. T.; Tjeng L. H., Electronic and magnetic properties of the kagome systems $YBaCo_4O_7$ and $YBaCo_3MO_7$ (M=Al, Fe). *Phys. Rev. B.* **2009**, *80*, 085111.
45. Hu, Z.; Wu, H.; Haverkort, M. W.; Hsieh, H. H.; Lin, H. -J.; Lorenz, T.; Baier, J.; Reichl, A.; Bonn, I.; Felser, C.; Tanaka, A.; Chen, C. T.; Tjeng, L. H., Different Look at the Spin State of Co^{3+} Ions in a CoO_5 Pyramidal Coordination. *Phys. Rev. Lett.* **2004**, *92*, 207402.
46. Mandziak, A.; Soria, G. D.; Prieto, J. E.; Prieto, P.; Granados-Miralles, C.; Quesada, A.; Foerster, M.; Aballe, L.; de la Figuera, J., Tuning the Néel temperature in an antiferromagnet: the case of $Ni_xCo_{1-x}O$ microstructures. *Sci. Rep.* **2019**, *9*, 13584.
47. Singh, V. R.; Sakamoto, Y.; Kataoka, T.; Kobayashi, M.; Yamazaki, Y.; Fujimori, A.; Chang, F.-H.; Huang, D.-J.;. Lin, H.-J; Chen, C. T.; Toyosaki, H.; Fukumura, T.; Kawasaki, Bulk and surface magnetization of Co atoms in rutile $Ti_{1-x}Co_xO_{2-\delta}$ thin films revealed by x-ray magnetic circular dichroism. M., *J. Phys.: Condens. Matter.* **2011**, *23*, 176001.
48. Thole, B. T.; Carra, P.; Sette, F.; van der Laan, G., X-ray circular dichroism as a probe of orbital magnetization. *Phys. Rev. Lett.* **1992**, *68*, 1943-1946.
49. Carra, P.; Thole, B. T.; Altarelli, M.; Wang, X., X-ray circular dichroism and local magnetic fields. *Phys. Rev. Lett.* **1993**, *70(5)*, 694-697.
50. Hermanns, C. F.; Bernien, M.; Krüger, A.; Walter, W.; Chang, Y.-M.; Weschke, E.; Kuch, W., Huge magnetically coupled orbital moments of Co porphyrin molecules and their control by CO adsorption. *Phys. Rev. B* **2013**, *88*, 104420.
51. Gambardella, P.; Dhesi, S. S.; Gardonio, S.; Grazioli, C.; Ohresser, P.; Carbone, C., *Phys. Rev. Lett.* **2002**, *88*, 047202.

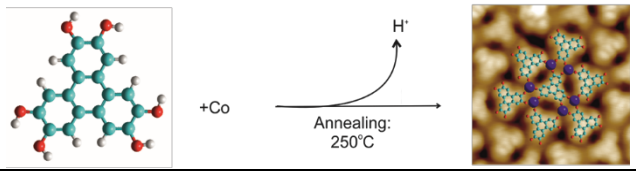
+Co
H+
Annealing:
250°C